Revealing 3D Orientation and the Interplay between Plasmons and Interband Transitions for Single Gold Bipyramids by Photoluminescence Excitation Pattern Imaging

Quan Liu,[1,2] Dandan Ge,[2] Frank Wackenhut,[1,4] Caitlin D. Coplan,[3] Charles Cherqui,[3] Marc Brecht,[1,4] Xiao-Min Lin,[5] George C. Schatz,[3] Richard D. Schaller,[3,5] Pierre-Michel Adam,[2] Renaud Bachelot[2,] and Alfred J. Meixner[1,*]*

[1] Institute of Physical and Theoretical Chemistry, Eberhard Karls University Tübingen, Auf der Morgenstelle 18, 72076 Tübingen, Germany

[2] Laboratoire Lumière, nanomatériaux & nanotechnologies − L2n and CNRS ERL 7004, Universitéde Technologie de Troyes, 10000 Troyes, France

[3] Department of Chemistry, Northwestern University, Evanston, Illinois 60208, United States

[4] Reutlingen Research Institute, Process Analysis and Technology (PA&T), Reutlingen University, Alteburgstraße 150, 72762 Reutlingen, Germany

[5] Center for Nanoscale Materials, Argonne National Laboratory, Lemont, Illinois 60439, United States

ABSTRACT: Gold bipyramids (AuBPs) attract significant attention due to the large enhancement of the electric field around their sharp tips and well-defined tunability of their plasmon resonances. Excitation patterns of single AuBPs are recorded using raster-scanning confocal microscopy combined with radially and azimuthally polarized laser beams. Photoluminescence spectra (PL) and excitation patterns of the same AuBP are acquired with three different excitation wavelengths. The isotropic excitation patterns suggest that the AuBPs are mainly excited by interband transitions with 488/530 nm radiation, while excitation patterns created with a 633 nm laser exhibit a double lobed shape that indicates a single dipole excitation process associated with the longitudinal plasmon resonance mode. We are able to determine the three-dimensional orientation of single AuBPs nonperturbatively by comparing experimental patterns with theoretical simulations. The asymmetric patterns show that the AuBPs are lying on the substrate with an out-of-plane tilt angle of around 10° to 15°.

TOC GRAPHICS

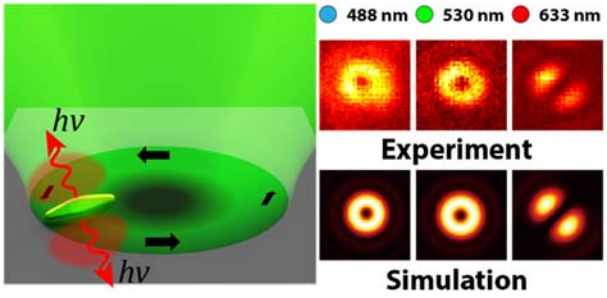

KEYWORDS: gold bipyramid, plasmon resonance, photoluminescence, higher order laser modes

INTRODUCTION

Noble metal nanostructures have been widely studied in the last decades, since they are ideally suited to confine incident light to volumes much smaller than the optical wavelength.[1–4] The same effect can be utilized for increasing the efficiency of light emission from nanostructures.[5] The ability to confine light into an intense near-field is due to localized plasmon resonances (LPR), which are a coherent oscillation of the conduction band electrons in these structures. The LPR are tunable over a large wavelength range since they sensitively depend on the size, shape, material composition, and surrounding dielectric medium of the nanostructures.[6–9] Hence, tunable plasmonic nanostructures play an important role for a variety of applications. For example, surface enhanced Raman spectroscopy (SERS) relies on the large amplification of the local electromagnetic field through sharp protrusions and small gaps,[10,11] or nanoantennas[2,5] which are designed for capturing and localizing energy from radiation into small subwavelength volumes or directional emission from the near-field to the far-field based on their structural anisotropy. Other applications, such as nano-light sources[12–15] and nonlinear optics,[16,17] can benefit from both enhanced absorption and emission processes.

Anisotropic gold nanoparticles, such as nanorods, are especially interesting due to the simple structure with high tunability of their plasmonic properties, hence they have been the subject of many studies.[4,18–20] Another anisotropic nanoparticle shape, the gold nanobipyramid (AuBP), is drawing growing attention for different possible applications.[21,22] A review highlights the fascinating plasmonic properties, growth methods and plasmonic applications of AuBPs can be found in [23]. The tunability of the optical properties of a AuBP is similar to a nanorod,[24] while

offering larger localized field enhancement due to sharper tips compared to nanorods. Compared to nanorods, AuBPs possess narrower plasmonic resonances,[25] higher shape uniformity, larger local field enhancement and instinctive asymmetric configuration on the supporting surface.[26,27] Despite the synthesis difficulty, new methods have enabled us to produce AuBPs with number percentages approaching 100%.[27,28] Fascinating applications, such as a prototyped biological application of a single molecule immunoassay[29] and a general experimental methodology[22] for single-molecule SERS, heavily rely on the large near-field enhancements located at the sharp tips of the AuBPs. Thus, it is important to characterize the scattering and photoluminescence properties of the AuBPs nonperturbatively and relate them to their orientation and the location of the tips.

In most cases, white light scattering is used to characterize the plasmonic properties of nanostructures. Scattering-based methods, such as defocused dark-field imaging,[30] back focal plane imaging,[31] interferometric scattering microscopy[32,33] and direct phase mapping[34] are utilized to distinguish the geometrical properties of nanoparticles. However, scattering methods suffer from a scattering background that originates from impurities and interfaces, which is especially problematic in biological applications. The scattering background can be circumvented by photothermal microscopy,[18,35] which is based on absorption of the nanoparticles. Nevertheless, thermal reshaping and melting is problematic, particularly for small nanostructure features due to their high surface energies. Surface plasmon enhanced photoluminescence (PL)[3,19,36,37] offers an alternative way to probe the properties of nanoparticles.

Raster-scanning confocal microscopy combined with the use of higher order laser beams has been used to characterize the scattering[38–40] or PL[37,41] signal of individual nanoparticles. In contrast to a linear polarized Gaussian beam, higher order laser beams offer symmetric electric

focus fields in all spatial directions, enabling to excite nanoparticles with any spatial orientation. This symmetry of the out-of-plane and in-plane components of the excitation field allows easy interpretation of the results. Furthermore, this approach allows to distinguish between different particle shapes, such as nanosphere, nanorod, or nanotriangles[39] due to different scattering patterns for each structure. The variation of excitation patterns has been correlated with three-dimensional orientation of a single nanorod fixed in a polymer matrix with an uncertainty of 5°.[41]

In this work, we report a detailed characterization of the scattering and PL properties of AuBPs deposited on an indium tin oxide (ITO) substrate on the single particle level. Raster-scanning confocal microscopy combined with azimuthally or radially polarized doughnut modes is used to map the three-dimensional orientation of single AuBPs. Additionally, taking advantage of the wavelength dependence of the optical properties of AuBPs allows us to investigate the origin of the PL in AuBPs. The isotropic excitation patterns suggest that the AuBPs are mainly excited by interband transitions with 488/530 nm radiation, while excitation patterns created with a 633 nm laser exhibit a double lobed shape that indicates a single dipole excitation process associated with the longitudinal plasmon resonance mode.

METHODS

AuBP preparation. AuBPs are synthesized using a seed-mediated growth method, described in detail in [26]. The first synthetic step is the growth of the gold seeds. $HAuCl_4$ is reduced using a basic $NaBH_4$ solution in the presence of citric acid, all in an aqueous CTAC solution. The second synthetic step is the growth of the bipyramids, where a more concentrated $HAuCl_4$ solution is added to an aqueous CTAB solution with $AgNO_3$. 8-hydroxyquinoline (HQL) is then added to this solution and is rapidly stirred for one minute. After this, a variable amount of the

Au seeds is then added, which determines the aspect ratio of the resultant bipyramids. This reaction was left in a 30°C water bath for two hours. This solution was centrifuged twice at 8000 rpm for 10 minutes to remove excess surfactant and was redispersed in milliQ (18.2 MOhm) water to obtain a diluted solution. 3 μL of the dilution was drop-cast on a cleaned ITO glass. The glass was rinsed after 15 minutes with water then ethanol, and dried under nitrogen flow.

AFM and SEM measurements. The morphologies of AuBPs were imaged using a Scanning Electron Microscope (SEM, Hitachi SU-8030) under an accelerating voltage of 2 kV to avoid sample damage. The AuBP were also characterized by atomic force microscopy (AFM) with the Bruker Dimension Icon in Peak Force tapping mode using standard SCANASYST-AIR silicon nitride tips.

Darkfield scattering. Darkfield (DF) spectra were measured with a commercial inverted microscope (IX71, Olympus) coupled to a spectrometer (Shamrock SR-303i with iDus CCD camera). White light from a halogen lamp is focused on the sample using a variable NA (0.7–0.9) darkfield condenser, and scattered light is collected using a 40 × 0.6 NA objective. Alignment of the isolated single AuBP is carried out by first aligning the center of the AuBP with the entrance slit of the spectrometer and then narrowing the slit until the detection area only contains the AuBP of interest. Multi-track mode was used to achieve spectral measurements of the individual bipyramids.

Photoluminescence measurements. PL excitation patterns and spectra were measured with a home built scanning confocal microscope[37] with different excitation wavelengths (488 nm, pulsed, D-C-485, PicoQuant; 530 nm, pulsed/CW, LDH-P-FA-530L, PicoQuant; 633 nm, CW). The formation and use of azimuthally (APDM) and radially polarized (RPDM) doughnut modes and their inhomogeneous field intensity distribution and polarization in the focal volume of a

high numerical aperture lens are described in ref. [42]. The practical advantage of APDM and RPDM for confocal single nanoparticle imaging and spectroscopy is that the polarization in the focal field has strict cylindrical symmetry and provides excitation patterns that directly reveal the three-dimensional orientation of the polarizability axes or transition dipole moment of a nanoparticle or single molecule. In short for an APDM the electric field is transversal and forms an azimuthally polarized doughnut shaped intensity pattern around the optical axis. For an RPDM the center part of the focal field is oriented along the optical axis (it is longitudinally polarized). It is surrounded by a radially polarized doughnut shaped field. The APDM and RPDM are generated by a commercial mode converter (polarization converter, Arcoptix). The excitation laser was focused on the sample by a high numerical aperture (NA = 1.46, 100×, Carl Zeiss) oil objective lens. The fluorescence signal was collected by the same objective lens and sent to avalanche photodiodes (APDs) or a spectrometer (Acton SP-2500i, Princeton Instruments). The sample is carefully fixed on a piezo stage (P-527.3CL, Physik Instruments) via a magnet to avoid spatial drift. The angular dependence of PL signal is obtained with a linearly polarized excitation laser (633 nm) by rotating a linear polarizer placed in front of the detector.

RESULTS AND DISCUSSION

Figure 1a) shows a typical AFM image of an AuBP. A topography cross-section profile along the white dashed line and a SEM image of the same particle are presented on the right side of Figure 1a). From the cross-section profile, it is evident that the AuBP is not lying flat on the substrate, but is slightly tilted with an angle ~10° with respect to the substrate plane. The boundary line of the AuBP obtained from the SEM image is overlapped with the AFM topography cross-section profile as a guide to the eye. The good fit of the two profiles indicates the high rotational symmetry of the AuBP. The size distribution obtained from SEM images of

the short (green) and long (red) axes of 100 AuBPs are shown in Figure 1b). The average length of the AuBP is 116.6±4.45 nm and 46.8±4.10 nm for the width of the AuBP. Inset in Fig. 1b) shows a representative dark field scattering spectrum for a single AuBP. Two distinct plasmonic modes at 556 nm and 717 nm are assigned to the short and long axis plasmon resonance, also known as the transversal plasmon resonance (TPR) and longitudinal plasmon resonance (LPR), respectively (in agreement with plane wave excited scattering and electric field computations, shown in Figure S1 and Figure S2).

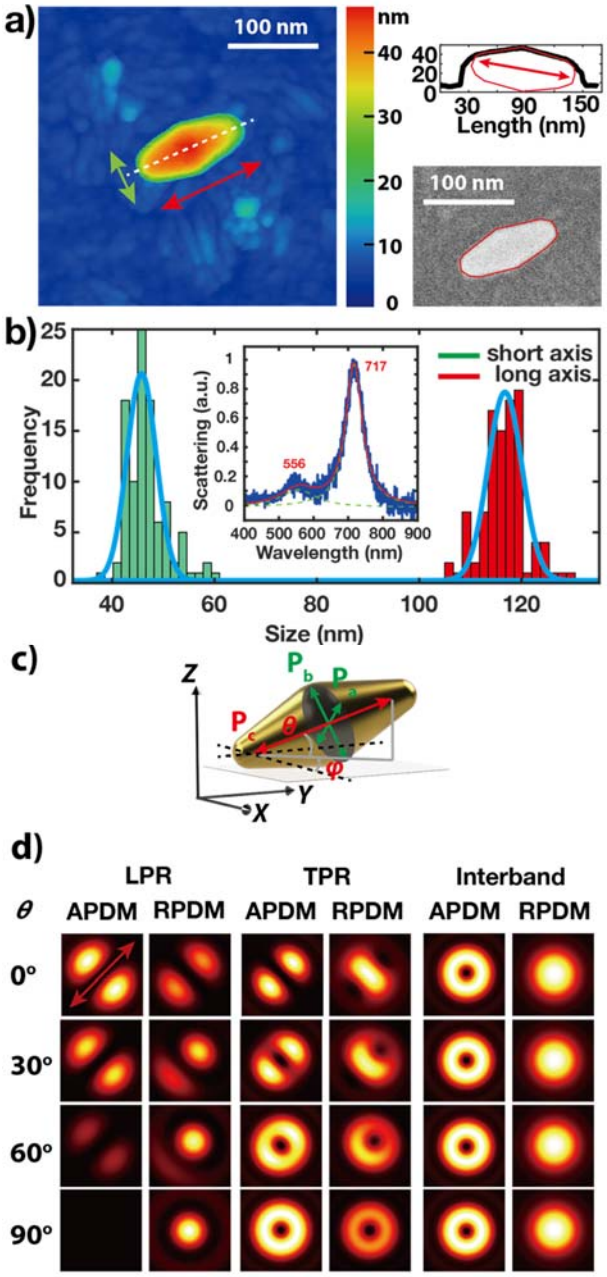

Figure.1 a) AFM image of a single gold nanobipyramid (AuBP) with a scanning range of 330 nm ×330 nm. The arrows indicate the in-plane direction of long (red) and short (green) axis. The right side shows a topography cross-section profile along the white dashed line and a SEM image of the same AuBP. The SEM boundary line of the AuBP is overlapped with an AFM topography cross-section profile. b) Size distribution of 100 AuBPs analyzed from SEM images. The

average length of the AuBP is 116.6±4.45 nm and 46.8±4.10 nm for the width of the AuBP. c) A scheme defining the orientation of the AuBP, the green and red arrows indicate the orientation of transverse plasmon resonance (TPR) and longitudinal plasmon resonance (LPR) with the respective polarizabilities $\mathbf{P_a}$, $\mathbf{P_b}$ and $\mathbf{P_c}$. The in-plane angle and out-of-plane angle are ϕ and θ, respectively. d) Theoretical excitation patterns calculated for a single AuBP with different out-of-plane angles raster scanned through the field intensity distribution of a tightly focused azimuthally polarized (APDM) and radially polarized (RPDM) laser beam. The three different features correspond to the LPR excited at 633 nm, the TPR excited at 530 nm and the interband transitions excited at 488 nm.

For the interpretation of the measured spectral patterns obtained by scanning a single AuBP through the highly confined field intensity distribution in the focal plane of an azimuthally or radially polarized doughnut mode (APDM and RPDM), we start our analysis with the theoretical excitation patterns.[41,43,44] The PL intensity is proportional to the square of the polarizability tensor $\hat{\alpha}$ times the amplitude of the electric field component of the excitation field $\boldsymbol{E}_{exc}$ and can be described as,[45]

$$I \propto |\hat{\boldsymbol{\alpha}} \cdot \boldsymbol{E}_{exc}|^2.$$

Analogous to nanorods,[3,19,35,46,47] the polarizability tensor $\hat{\boldsymbol{\alpha}}$ of the AuBP can be modeled by three orthogonal dipole components $\mathbf{P_a}$, $\mathbf{P_b}$ and $\mathbf{P_c}$ aligned along the main axes of the AuBP as shown in Fig. 1c), where $\mathbf{P_a}$, $\mathbf{P_b}$ are proportional to the polarizabilities of the short axes and describe the TPR and $\mathbf{P_c}$ describes the LPR. The interband transitions[48] can also be included by introducing an extra term into the diagonal elements of $\hat{\boldsymbol{\alpha}}$. The white-light scattering spectrum (Fig. 1b)) serves as a good characterization of the polarizability of the TPR and the LPR.[26] Due

to their spectral separation, TPR and LPR can be excited individually, while interband transition must be excited with shorter wavelength (488 nm and 530 nm) radiation. Fig. 1d) shows simulated excitation patterns of AuBPs with different out-of-plane angles excited with APDM and RPDM laser beams. Clear differences in the pattern shapes allow to distinguish between PL caused by the plasmon resonances or by the interband transition. The symmetry of the excitation patterns associated with the interband transition is caused by the isotropic polarizability tensor. We note that the out-of-plane orientation of a single AuBP can be unambiguously determined via RPDM excitation.

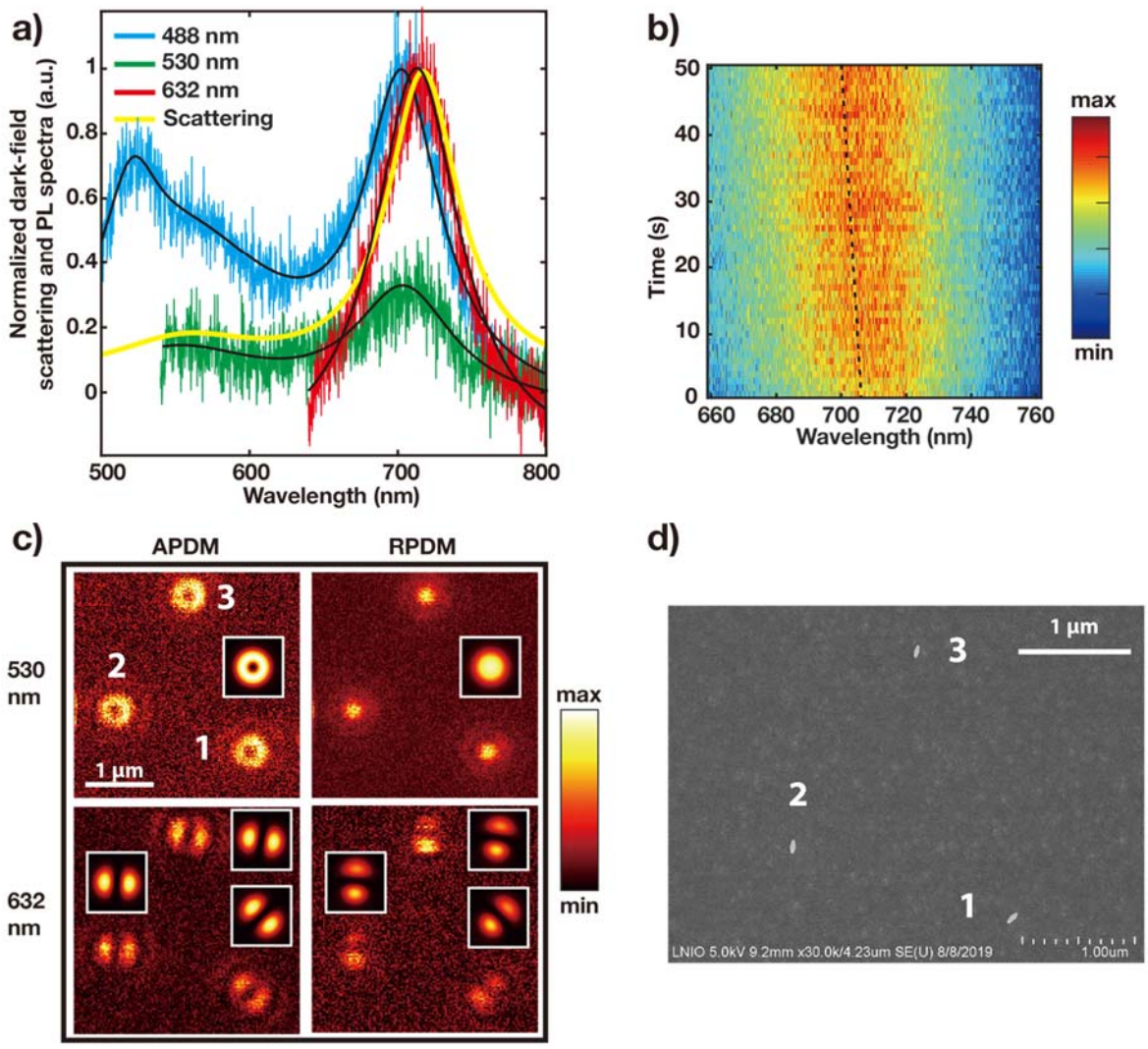

Figure.2 a) Photoluminescence (PL) spectra of AuBP 1 in d) that were obtained using different excitation wavelengths. The excitation lasers power was set to 25 µW in front of the objective. The solid black curves are Lorentzian fits. The darkfield scattering spectrum is also plotted as the solid yellow line. b) Time series of PL spectra of AuBP 1 acquired with 530 nm excitation. c) PL excitation patterns of single AuBPs excited at 530 nm (top row) and 633 nm (bottom row) using APDM and RPDM laser beams. Inset figures are simulated patterns. d) SEM image of same AuBPs.

Figure 2a) shows PL spectra of the same single AuBP excited at three different wavelengths (488 nm blue line, 530 nm green line, 633 nm red line). One pronounced peak around 710 nm appears for all excitation wavelengths (700 nm for 488 nm excitation, 703 nm for 530 nm excitation, and 714 nm for 633 nm excitation) and is assigned to LPR-induced emission. There is a blue-shift (~10 nm) of the LPR-induced emission relative to the DF scattering spectra (yellow line) when excited with 488 nm and 530 nm, while the PL spectrum obtained for 633 nm excitation overlaps with scattering spectra. This blue shift can be explained by the larger free electron densities available for the interband transitions[19,49,50] excited with 488 nm and 530 nm excitation. A second peak can be observed around 550 nm for 488 nm and 530 nm excitation wavelengths and can be assigned to TPR induced emission. The third peak around 522 nm appears for excitation at 488 nm and is caused by interband radiative relaxation near the *L* symmetry point.[36,51] The agreement between the PL excited at 633 nm with dark field scattering spectrum also proves that the AuBP doesn't reshape or is partially melted during the measurement. Figure 2b) is a time series of PL spectra of AuBP 1 acquired with 530 nm excitation over a time period of 50 s. The intensity of the spectra is stable over a long time period, while the peak of PL spectra blue-shifts from 704 nm to 700 nm according to Lorentzian fits. This slight blue shift could be a thermal effect due to the change of the refractive index caused by continued laser excitation.[52] The thermal effect or damage to the AuBP is unlikely to be responsible for the ~10 nm difference between dark field scattering and LPR induced emission excited at 488 nm and 530 nm, however, as the PL spectrum using 633 nm excitation is acquired after the short wavelength excitation.

Photoluminescence of gold is in general very low with a quantum yield on the order of 10^{-10} and was first reported by Mooradian in 1968,[53] and interpreted as the radiative recombination of

free electrons in the *sp*-conduction band with excited *d*-band holes caused by interband transitions. This is different for gold nanoparticles compared to films since the plasmon-mediated photoluminescence is one of the important emission routes[3,36,45,46] as shown by the pronounced peaks observed in PL in Figure 2a) and the quantum yield can increase by several orders of magnitude.[19,35] Electron-hole pairs can be converted into plasmonic oscillations after a fast dephasing (~1 ps) process,[36,54] which can subsequently radiatively relax. Altogether, these emission processes lead to an emission spectrum, which is dominated by the plasmon modes as illustrated in Figure 2a) using 488 nm and 530 nm excitation.

Figure 2c) shows excitation patterns of the single AuBPs shown in Figure 2d) excited at 530 nm (top row) and 633 nm (bottom row) using APDM and RPDM laser beams. The pattern shape strongly depends on the excitation wavelength and excitation doughnut mode. Even though both TPR mode and interband transitions can be excited by 530 nm photons, we can exclude that TPR excitation significantly contributes to the PL emission, since the pattern shapes indicate an isotropic excitation and reflecting the electric field distribution of the focused beam.[55] One might argue that LPR could also be excited directly by the 530 nm laser and thus cause an isotropic excitation pattern. However, it can be excluded by the fact that excitation patterns acquired with only red channel (634 nm long pass) remain isotropic (see Figure 3c)). If the LPR is, at least partially, directly excited, the pattern shape in the red channel should be anisotropic. The isotropic excitation process suggests that the AuBPs are mainly excited by interband transitions, which give symmetric ring like patterns as can be seen in Figure 1d). The fast dephasing time[37] of the TPR mode may explain the weak contribution of TPR excitation to the PL. Excitation patterns using the 633 nm laser always have a double lobed shape, which is a proof of a single dipole excitation process showing that only the LPR mode is excited. Inset

figures are the theoretical fits of the excitation patterns. The orientation of the double lobes using the APDM correlates with the in-plane orientation of the AuBP, which perfectly agrees with the SEM image in Figure 2d). Asymmetric patterns acquired with RPDM show that the AuBPs are lying on the substrate with an out-plane angle around 10° to 15°, which is in agreement with the AFM cross-sectional profile in Figure 1a).

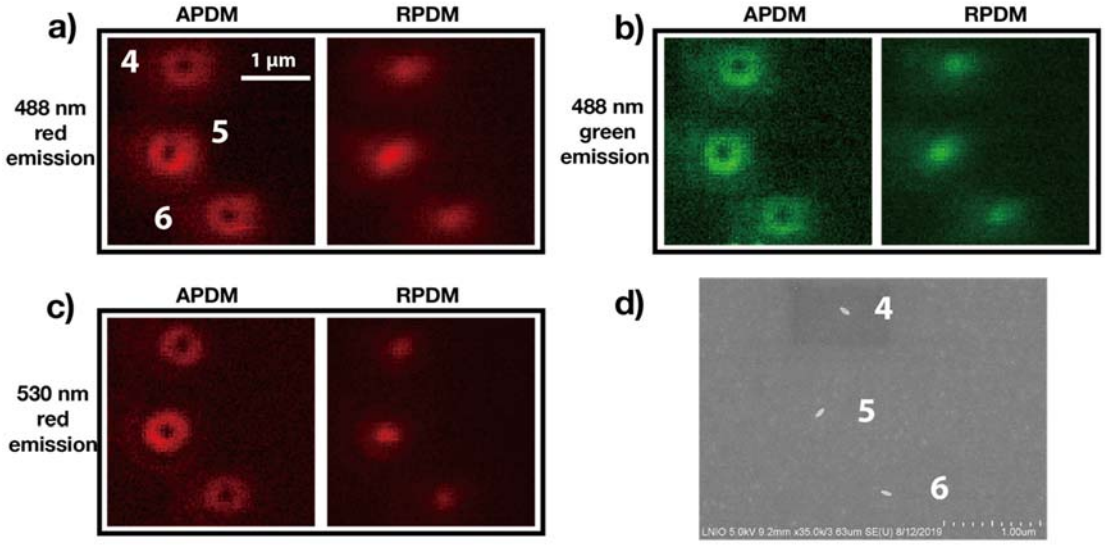

Figure.3 a-c) PL excitation patterns of single AuBP excited at 488 nm (a/b) and 530 nm (c) using APDM and RPDM laser beams. Emission was separated into emission below (green channel) and above (red channel) 633 nm to distinguish the emission from LPR, TPR and interband transitions. (d) SEM image of the same area is shown in a-c).

To further confirm that interband transitions are accountable for the isotropic excitation patterns, we scanned AuBP 4-6 at 488 nm using APDM and RPDM laser beams, which mainly excites interband transitions. When performing simulations for interband transitions in Figure 1d), we have assumed that emission polarization is not related to the excitation polarization, i.e. interband transitions created free electron hole pairs undergo a fast dephasing process, then can

go through interband, TPR or LPR radiative relaxation. To address this, LPR and TPR induced emission are separated into a green and red channel by different filters (634 nm long pass, 633 nm short pass). If relaxation path is related to specified excitation polarization, pattern shapes in the red and green channel should be different. As shown in Figure 3, excitation patterns of AuBP 4-6 remain isotropic for both green and red channel, showing that the excitation process is isotropic regardless of the detected emission wavelength. This shows that excitation of electron hole pairs is dominant and that they decay radiatively or excite plasmons.

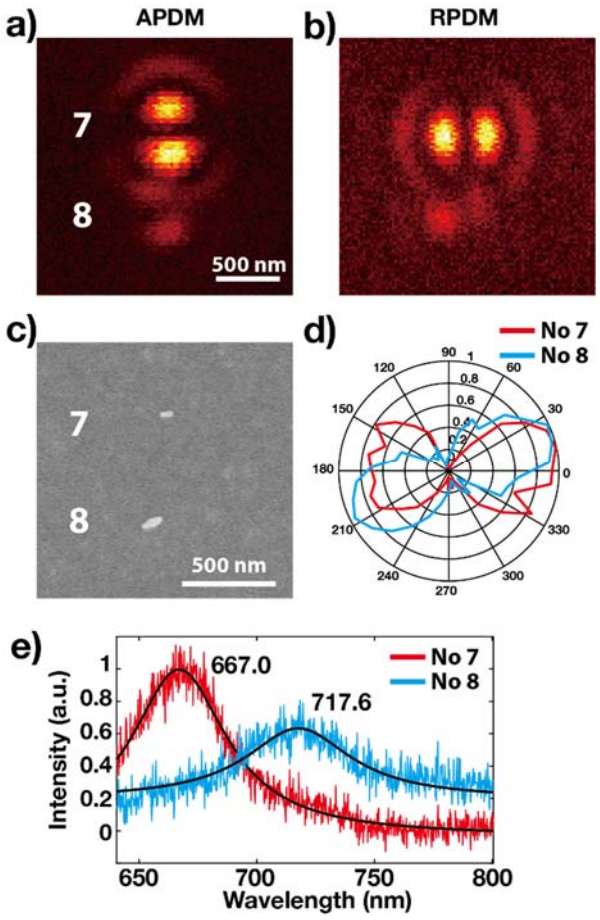

Figure.4 a-b) PL excitation patterns of a single gold nanorod (particle 7) and AuBP (particle 8), excited at 633 nm using APDM and RPDM laser beam. c) SEM image of the same area. The in-plane angle of AuBP and nanorod shows excellent agreement between excitation patterns and the

SEM image. d) Angular dependence of PL for AuBP and gold nanorod using 633 nm linear polarized excitation. e) PL spectra of single gold nanorod (particle 7) and AuBP (particle 8) that were excited at 633 nm. The solid black curves are Lorentzian fits.

We also compare the excitation patterns of an AuBP with a gold nanorod. In Figure 4a), both nanoparticles show symmetric double lobe patterns excited with APDM at 633 nm. The in-plane orientations of the double-lobed patterns perfectly agree with the SEM image in Figure 4c). Asymmetric patterns of an AuBP excited with the RPDM in Figure 4b) reveals an out-of-plane tilt, while the gold nanorod lies flat on the substrate and produces a symmetric excitation pattern. The difference of PL intensity is caused by the spectral peak positions of the LPR of the nanorod. It is closer to the excitation wavelength of 633 nm, as can be seen by the PL spectra in Figure 4e), hence the nanorod has a stronger resonance enhancement. The PL polarization of both nanostructures, acquired by rotating a linear polarizer in front of the detector, exhibits dipole-like character using 633 nm linear polarized excitation, and emission dipoles are in the same direction as excitation dipoles. This result again suggests that only the LPR is involved with 633 nm excitation.

CONCLUSIONS

In summary, we show how to determine the three-dimensional orientation of a single AuBP using 633 nm APDM and RPDM excitation, which is highly consistent with the results from SEM and AFM techniques. The origin of PL generated by a single AuBP can be unambiguously revealed using higher order laser modes (APDM and RPDM) excitation at different wavelengths. Compared with theoretical simulations, we demonstrated that interband transitions dominate PL signals when using 488 and 530 nm excitation sources. This distinction between excitation

sources and resultant PL signals is due to the differences in emission pathways. For the 633 nm excitation the main excitation process is a direct excitation of the LPR, whereas the interband transition dominates for the 488 and 530 nm excitation sources. Both excitation and emission processes of a single AuBP with 633 nm laser excitation can be well modeled as a single LPR dipole. Raster scanning confocal microscopy combined with higher order laser modes provides an effective tool to probe the three-dimensional orientation of nanoparticles and, thus, the orientation of tightly confined hot-spots. This is important for all applications that rely on large local field enhancement, and suggests potential for future applications in biology and materials science.

ASSOCIATED CONTENT

Supporting Information

The Supporting Information is available free of charge on the ACS Publications website.

Modeling and simulations (PDF)

AUTHOR INFORMATION

Corresponding Author

Renaud Bachelot − Laboratoire Lumière, nanomatériaux & nanotechnologies − L2n and CNRS ERL 7004, Universitéde Technologie de Troyes, 10000 Troyes, France; orcid.org/ 0000-0003-1847-5787; Email: renaud.bachelot@utt.fr

Alfred J. Meixner − Institute of Physical and Theoretical Chemistry, Eberhard Karls University Tübingen, 72076 Tübingen, Germany; orcid.org/0000-0002-0187-2906; Email: alfred.meixner@uni-tuebingen.de

Authors

Quan Liu − Institute of Physical and Theoretical Chemistry, Eberhard Karls University Tübingen, 72076 Tübingen, Germany; Laboratoire Lumière, nanomatériaux & nanotechnologies − L2n and CNRS ERL 7004, Université de Technologie de Troyes, 10000 Troyes, France

Dandan Ge − Laboratoire Lumière, nanomatériaux & nanotechnologies − L2n and CNRS ERL 7004, Universitéde Technologie de Troyes, 10000 Troyes, France

Frank Wackenhut − Institute of Physical and Theoretical Chemistry, Eberhard Karls University Tübingen, 72076 Tübingen, Germany; Reutlingen Research Institute, Process Analysis and Technology (PA&T), Reutlingen University, Alteburgstraße 150, 72762 Reutlingen, Germany

Caitlin D. Coplan - Department of Chemistry, Northwestern University, Evanston, Illinois 60208, United States

Charles Cherqui − Department of Chemistry, Northwestern University, Evanston, Illinois 60208, United States

Marc Brecht − Institute of Physical and Theoretical Chemistry, Eberhard Karls University Tübingen, 72076 Tübingen, Germany; Reutlingen Research Institute, Process Analysis and Technology (PA&T), Reutlingen University, Alteburgstraße 150, 72762 Reutlingen, Germany

Xiao-Min Lin − Center for Nanoscale Materials, Argonne National Laboratory, Lemont, Illinois 60439, United States

George C. Schatz − Department of Chemistry, Northwestern University, Evanston, Illinois 60208, United States

Richard D. Schaller − Department of Chemistry, Northwestern University, Evanston, Illinois 60208, United States; Center for Nanoscale Materials, Argonne National Laboratory, Lemont, Illinois 60439, United States

Pierre-Michel Adam − Laboratoire Lumière, nanomatériaux & nanotechnologies − L2n and CNRS ERL 7004, Universitéde Technologie de Troyes, 10000 Troyes, France

Notes

The authors declare no competing financial interest.

ACKNOWLEDGMENTS:

Q.L. and D.G. contributed equally to this work. The authors gratefully acknowledge funding by the German Research Foundation (DFG, ME 1600/13-3) and the Funding of China Scholarship Council (CSC). CDC, CC, GCS, and RDS acknowledge support by the Ultrafast Initiative of the U. S. Department of Energy, Office of Science, Office of Basic Energy Sciences, through Argonne National Laboratory under Contract No. DE-AC02-06CH11357. This work was performed within the framework of the Graduate School NANO-PHOT (École Universitaire de Recherche, contract ANR-18-EURE-0013) and, in part, at the Center for Nanoscale Materials,

a U.S. Department of Energy Office of Science User Facility, and supported by the U.S. Department of Energy, Office of Science, under Contract No. DE-AC02-06CH11357.

REFERENCE:

(1) Kelly, K. L.; Coronado, E.; Zhao, L. L.; Schatz, G. C. The Optical Properties of Metal Nanoparticles: The Influence of Size, Shape, and Dielectric Environment, *J. Phys. Chem. B*, **2003**, *107*, 668–677, DOI:10.1021/jp026731y.

(2) Giannini, V.; Fernández-Domínguez, A. I.; Heck, S. C.; Maier, S. A. Plasmonic Nanoantennas: Fundamentals and Their Use in Controlling the Radiative Properties of Nanoemitters, *Chem. Rev.*, **2011**, *111*, 3888–3912, DOI:10.1021/cr1002672.

(3) Bouhelier, A.; Bachelot, R.; Lerondel, G.; Kostcheev, S.; Royer, P.; Wiederrecht, G. P. Surface Plasmon Characteristics of Tunable Photoluminescence in Single Gold Nanorods, *Phys. Rev. Lett.*, **2005**, *95*, 267405, DOI:10.1103/PhysRevLett.95.267405.

(4) Link, S.; El-Sayed, M. A. Spectral Properties and Relaxation Dynamics of Surface Plasmon Electronic Oscillations in Gold and Silver Nanodots and Nanorods, *J. Phys. Chem. B*, **1999**, *103*, 8410–8426, DOI:10.1021/jp9917648.

(5) Novotny, L.; van Hulst, N. Antennas for Light, *Nat. Photonics*, **2011**, *5*, 83–90, DOI:10.1038/nphoton.2010.237.

(6) Hayashi, S.; Okamoto, T. Plasmonics: Visit the Past to Know the Future, *J. Phys. Appl. Phys.*, **2012**, *45*, 433001, DOI:10.1088/0022-3727/45/43/433001.

(7) Mock, J. J.; Hill, R. T.; Degiron, A.; Zauscher, S.; Chilkoti, A.; Smith, D. R. Distance-Dependent Plasmon Resonant Coupling between a Gold Nanoparticle and Gold Film, *Nano Lett.*, **2008**, *8*, 2245–2252, DOI:10.1021/nl080872f.

(8) Tan, B. J. Y.; Sow, C. H.; Koh, T. S.; Chin, K. C.; Wee, A. T. S.; Ong, C. K. Fabrication of Size-Tunable Gold Nanoparticles Array with Nanosphere Lithography, Reactive Ion Etching, and Thermal Annealing, *J. Phys. Chem. B*, **2005**, *109*, 11100–11109, DOI:10.1021/jp045172n.

(9) Gonçalves, M. R. Plasmonic Nanoparticles: Fabrication, Simulation and Experiments, *J. Phys. Appl. Phys.*, **2014**, *47*, 213001, DOI:10.1088/0022-3727/47/21/213001.

(10) Mohamed, M. B.; Volkov, V.; Link, S.; El-Sayed, M. A. The `lightning' Gold Nanorods: Fluorescence Enhancement of over a Million Compared to the Gold Metal, *Chem. Phys. Lett.*, **2000**, *317*, 517–523, DOI:10.1016/S0009-2614(99)01414-1.

(11) Maier, S. A. Plasmonic Field Enhancement and SERS in the Effective Mode Volume Picture, *Opt. Express*, **2006**, *14*, 1957–1964, DOI:10.1364/OE.14.001957.

(12) Hugall, J. T.; Singh, A.; van Hulst, N. F. Plasmonic Cavity Coupling, *ACS Photonics*, **2018**, *5*, 43–53, DOI:10.1021/acsphotonics.7b01139.

(13) Laux, F.; Bonod, N.; Gérard, D. Single Emitter Fluorescence Enhancement with Surface Lattice Resonances, *J. Phys. Chem. C*, **2017**, *121*, 13280–13289, DOI:10.1021/acs.jpcc.7b04207.

(14) Jäger, S.; Kern, A. M.; Hentschel, M.; Jäger, R.; Braun, K.; Zhang, D.; Giessen, H.; Meixner, A. J. Au Nanotip as Luminescent Near-Field Probe, *Nano Lett.*, **2013**, *13*, 3566–3570, DOI:10.1021/nl401173g.

(15) Reichenbach, P.; Horneber, A.; Gollmer, D. A.; Hille, A.; Mihaljevic, J.; Schäfer, C.; Kern, D. P.; Meixner, A. J.; Zhang, D.; Fleischer, M.; *et al.* Nonlinear Optical Point Light Sources through Field Enhancement at Metallic Nanocones, *Opt. Express*, **2014**, *22*, 15484–15501, DOI:10.1364/OE.22.015484.

(16) Wang, J.; Butet, J.; Baudrion, A.-L.; Horrer, A.; Lévêque, G.; Martin, O. J. F.; Meixner, A. J.; Fleischer, M.; Adam, P.-M.; Horneber, A.; *et al.* Direct Comparison of Second Harmonic Generation and Two-Photon Photoluminescence from Single Connected Gold Nanodimers, *J. Phys. Chem. C*, **2016**, *120*, 17699–17710, DOI:10.1021/acs.jpcc.6b04850.

(17) Hubert, C.; Billot, L.; Adam, P.-M.; Bachelot, R.; Royer, P.; Grand, J.; Gindre, D.; Dorkenoo, K. D.; Fort, A. Role of Surface Plasmon in Second Harmonic Generation from Gold Nanorods, *Appl. Phys. Lett.*, **2007**, *90*, 181105, DOI:10.1063/1.2734503.

(18) Chang, W.-S.; Ha, J. W.; Slaughter, L. S.; Link, S. Plasmonic Nanorod Absorbers as Orientation Sensors, *Proc. Natl. Acad. Sci.*, **2010**, *107*, 2781–2786, DOI:10.1073/pnas.0910127107.

(19) Fang, Y.; Chang, W.-S.; Willingham, B.; Swanglap, P.; Dominguez-Medina, S.; Link, S. Plasmon Emission Quantum Yield of Single Gold Nanorods as a Function of Aspect Ratio, *ACS Nano*, **2012**, *6*, 7177–7184, DOI:10.1021/nn3022469.

(20) Khatua, S.; Orrit, M. Probing, Sensing, and Fluorescence Enhancement with Single Gold Nanorods, *J. Phys. Chem. Lett.*, **2014**, *5*, 3000–3006, DOI:10.1021/jz501253j.

(21) Arenal, R.; Henrard, L.; Roiban, L.; Ersen, O.; Burgin, J.; Treguer-Delapierre, M. Local Plasmonic Studies on Individual Core–Shell Gold–Silver and Pure Gold Nano-Bipyramids, *J. Phys. Chem. C*, **2014**, *118*, 25643–25650, DOI:10.1021/jp5066105.

(22) Le Ru, E. C.; Grand, J.; Sow, I.; Somerville, W. R. C.; Etchegoin, P. G.; Treguer-Delapierre, M.; Charron, G.; Félidj, N.; Lévi, G.; Aubard, J. A Scheme for Detecting Every Single Target Molecule with Surface-Enhanced Raman Spectroscopy, *Nano Lett.*, **2011**, *11*, 5013–5019, DOI:10.1021/nl2030344.

(23) Chow, T. H.; Li, N.; Bai, X.; Zhuo, X.; Shao, L.; Wang, J. Gold Nanobipyramids: An Emerging and Versatile Type of Plasmonic Nanoparticles, *Acc. Chem. Res.*, **2019**, *52*, 2136–2146, DOI:10.1021/acs.accounts.9b00230.

(24) Liu, M.; Guyot-Sionnest, P. Mechanism of Silver(I)-Assisted Growth of Gold Nanorods and Bipyramids, *J. Phys. Chem. B*, **2005**, *109*, 22192–22200, DOI:10.1021/jp054808n.

(25) Kou, X.; Ni, W.; Tsung, C.-K.; Chan, K.; Lin, H.-Q.; Stucky, G. D.; Wang, J. Growth of Gold Bipyramids with Improved Yield and Their Curvature-Directed Oxidation, *Small*, **2007**, *3*, 2103–2113, DOI:10.1002/smll.200700379.

(26) Chateau, D.; Liotta, A.; Vadcard, F.; Navarro, J. R. G.; Chaput, F.; Lermé, J.; Lerouge, F.; Parola, S. From Gold Nanobipyramids to Nanojavelins for a Precise Tuning of the Plasmon Resonance to the Infrared Wavelengths: Experimental and Theoretical Aspects, *Nanoscale*, **2015**, *7*, 1934–1943, DOI:10.1039/C4NR06323F.

(27) Sánchez-Iglesias, A.; Winckelmans, N.; Altantzis, T.; Bals, S.; Grzelczak, M.; Liz-Marzán, L. M. High-Yield Seeded Growth of Monodisperse Pentatwinned Gold Nanoparticles through Thermally Induced Seed Twinning, *J. Am. Chem. Soc.*, **2017**, *139*, 107–110, DOI:10.1021/jacs.6b12143.

(28) Li, Q.; Zhuo, X.; Li, S.; Ruan, Q.; Xu, Q.-H.; Wang, J. Production of Monodisperse Gold Nanobipyramids with Number Percentages Approaching 100% and Evaluation of Their Plasmonic Properties, *Adv. Opt. Mater.*, **2015**, *3*, 801–812, DOI:10.1002/adom.201400505.

(29) Mayer, K. M.; Hao, F.; Lee, S.; Nordlander, P.; Hafner, J. H. A Single Molecule Immunoassay by Localized Surface Plasmon Resonance, *Nanotechnology*, **2010**, *21*, 255503, DOI:10.1088/0957-4484/21/25/255503.

(30) Xiao, L.; Qiao, Y.; He, Y.; Yeung, E. S. Three Dimensional Orientational Imaging of Nanoparticles with Darkfield Microscopy, *Anal. Chem.*, **2010**, *82*, 5268–5274, DOI:10.1021/ac1006848.

(31) Curto, A. G.; Taminiau, T. H.; Volpe, G.; Kreuzer, M. P.; Quidant, R.; van Hulst, N. F. Multipolar Radiation of Quantum Emitters with Nanowire Optical Antennas, *Nat. Commun.*, **2013**, *4*, DOI:10.1038/ncomms2769.

(32) Ortega-Arroyo, J.; Kukura, P. Interferometric Scattering Microscopy (ISCAT): New Frontiers in Ultrafast and Ultrasensitive Optical Microscopy, *Phys. Chem. Chem. Phys.*, **2012**, *14*, 15625–15636, DOI:10.1039/C2CP41013C.

(33) Lin, Y.-H.; Chang, W.-L.; Hsieh, C.-L. Shot-Noise Limited Localization of Single 20 Nm Gold Particles with Nanometer Spatial Precision within Microseconds, *Opt. Express*, **2014**, *22*, 9159–9170, DOI:10.1364/OE.22.009159.

(34) Hauler, O.; Wackenhut, F.; Jakob, L. A.; Stuhl, A.; Laible, F.; Fleischer, M.; Meixner, A. J.; Braun, K. Direct Phase Mapping of the Light Scattered by Single Plasmonic Nanoparticles, *Nanoscale*, **2020**, *12*, 1083–1090, DOI:10.1039/C9NR10358A.

(35) Yorulmaz, M.; Khatua, S.; Zijlstra, P.; Gaiduk, A.; Orrit, M. Luminescence Quantum Yield of Single Gold Nanorods, *Nano Lett.*, **2012**, *12*, 4385–4391, DOI:10.1021/nl302196a.

(36) Dulkeith, E.; Niedereichholz, T.; Klar, T. A.; Feldmann, J.; von Plessen, G.; Gittins, D. I.; Mayya, K. S.; Caruso, F. Plasmon Emission in Photoexcited Gold Nanoparticles, *Phys. Rev. B*, **2004**, *70*, 205424, DOI:10.1103/PhysRevB.70.205424.

(37) Wackenhut, F.; Failla, A. V.; Meixner, A. J. Multicolor Microscopy and Spectroscopy Reveals the Physics of the One-Photon Luminescence in Gold Nanorods, *J. Phys. Chem. C*, **2013**, *117*, 17870–17877, DOI:10.1021/jp407353r.

(38) Züchner, T.; Failla, A. V.; Steiner, M.; Meixner, A. J. Probing Dielectric Interfaces on the Nanoscale with Elastic Scattering Patterns of Single Gold Nanorods, *Opt. Express*, **2008**, *16*, 14635–14644, DOI:10.1364/OE.16.014635.

(39) Züchner, T.; Failla, A. V.; Hartschuh, A.; Meixner, A. J. A Novel Approach to Detect and Characterize the Scattering Patterns of Single Au Nanoparticles Using Confocal Microscopy, *J. Microsc.*, **2008**, *229*, 337–343, DOI:10.1111/j.1365-2818.2008.01910.x.

(40) Failla, A. V.; Qian, H.; Qian, H.; Hartschuh, A.; Meixner, A. J. Orientational Imaging of Subwavelength Au Particles with Higher Order Laser Modes, *Nano Lett.*, **2006**, *6*, 1374–1378, DOI:10.1021/nl0603404.

(41) Wackenhut, F.; Virgilio Failla, A.; Züchner, T.; Steiner, M.; Meixner, A. J. Three-Dimensional Photoluminescence Mapping and Emission Anisotropy of Single Gold Nanorods, *Appl. Phys. Lett.*, **2012**, *100*, 263102, DOI:10.1063/1.4729152.

(42) Züchner, T.; Failla, A. V.; Meixner, A. J. Light Microscopy with Doughnut Modes: A Concept to Detect, Characterize, and Manipulate Individual Nanoobjects, *Angew. Chem. Int. Ed.*, **2011**, *50*, 5274–5293, DOI:10.1002/anie.201005845.

(43) Novotny, L.; Beversluis, M. R.; Youngworth, K. S.; Brown, T. G. Longitudinal Field Modes Probed by Single Molecules, *Phys. Rev. Lett.*, **2001**, *86*, 5251–5254, DOI:10.1103/PhysRevLett.86.5251.

(44) Dorn, R.; Quabis, S.; Leuchs, G. Sharper Focus for a Radially Polarized Light Beam, *Phys. Rev. Lett.*, **2003**, *91*, 233901, DOI:10.1103/PhysRevLett.91.233901.

(45) Beversluis, M. R.; Bouhelier, A.; Novotny, L. Continuum Generation from Single Gold Nanostructures through Near-Field Mediated Intraband Transitions, *Phys. Rev. B*, **2003**, *68*, 115433, DOI:10.1103/PhysRevB.68.115433.

(46) Cai, Y.-Y.; Liu, J. G.; Tauzin, L. J.; Huang, D.; Sung, E.; Zhang, H.; Joplin, A.; Chang, W.-S.; Nordlander, P.; Link, S. Photoluminescence of Gold Nanorods: Purcell Effect Enhanced Emission from Hot Carriers, *ACS Nano*, **2018**, *12*, 976–985, DOI:10.1021/acsnano.7b07402.

(47) Tcherniak, A.; Dominguez-Medina, S.; Chang, W.-S.; Swanglap, P.; Slaughter, L. S.; Landes, C. F.; Link, S. One-Photon Plasmon Luminescence and Its Application to Correlation Spectroscopy as a Probe for Rotational and Translational Dynamics of Gold Nanorods, *J. Phys. Chem. C*, **2011**, *115*, 15938–15949, DOI:10.1021/jp206203s.

(48) Novotny, L.; Hecht, B. *Principles of Nano-Optics*, Cambridge University Press, 2nd edn., **2012**.

(49) Besteiro, L. V.; Kong, X.-T.; Wang, Z.; Hartland, G.; Govorov, A. O. Understanding Hot-Electron Generation and Plasmon Relaxation in Metal Nanocrystals: Quantum and Classical Mechanisms, *ACS Photonics*, **2017**, *4*, 2759–2781, DOI:10.1021/acsphotonics.7b00751.

(50) Binkowski, F.; Wu, T.; Lalanne, P.; Burger, S.; Govorov, A. O. Hot Electron Generation through Near-Field Excitation of Plasmonic Nanoresonators, *ACS Photonics*, **2021**, acsphotonics.1c00231, DOI:10.1021/acsphotonics.1c00231.

(51) Boyd, G. T.; Yu, Z. H.; Shen, Y. R. Photoinduced Luminescence from the Noble Metals and Its Enhancement on Roughened Surfaces, *Phys. Rev. B*, **1986**, *33*, 7923, DOI:10.1103/PhysRevB.33.7923.

(52) Kim, J.; Shrestha, S.; Souri, M.; Connell, J. G.; Park, S.; Seo, A. High-Temperature Optical Properties of Indium Tin Oxide Thin-Films, *Sci. Rep.*, **2020**, *10*, 12486, DOI:10.1038/s41598-020-69463-4.

(53) Mooradian, A. Photoluminescence of Metals, *Phys. Rev. Lett.*, **1969**, *22*, 185–187, DOI:10.1103/PhysRevLett.22.185.

(54) Zhang, X.; Huang, C.; Wang, M.; Huang, P.; He, X.; Wei, Z. Transient Localized Surface Plasmon Induced by Femtosecond Interband Excitation in Gold Nanoparticles, *Sci. Rep.*, **2018**, *8*, 10499, DOI:10.1038/s41598-018-28909-6.

(55) Fulmes, J.; Gollmer, D. A.; Jäger, S.; Schäfer, C.; Horrer, A.; Zhang, D.; Adam, P.-M.; Meixner, A. J.; Kern, D. P.; Fleischer, M. Mapping the Electric Field Distribution of Tightly Focused Cylindrical Vector Beams with Gold Nanorings, *Opt. Express*, **2018**, *26*, 14982, DOI:10.1364/OE.26.014982.